RESEARCH ARTICLE OPEN ACCESS

# Crystallization kinetics and phase transformation in amorphous $Fe_{74}Co_{10}B_{16}$ and $Fe_{67}Co_{18}B_{14}Si_1$ alloys

B. Bhanu Prasad
M.V.S.R. Engineering College, Nadergul, Hyderabad – 501 510.

**Abstract**
Crystallization kinetics and phase transformation studies have been carried out on amorphous $Fe_{74}Co_{10}B_{16}$ (S1) and $Fe_{67}Co_{18}B_{14}Si_1$ (S2) alloys using Mossbauer Spectroscopy (MS), Electrical Resistivity (ER), Differential Scanning Calorimetry(DSC), X-ray Diffraction(XRD) and Transmission Electron Microscopy(TEM) to determine the thermal stability. Results show that the transformation to an equilibrium crystalline state occurs through a two step process. Crystallization process is associated with precipitation of two or more phases which are magnetic in nature. From DSC curves, the activation energy of sample S2 has been calculated using Kissinger, Matusita-Sakka and Augis-Bennet methods and the average value is found to be 211 kJ/mol. The detected phases upon crystallization in the samples are α–(Fe-Co) and $(Fe\text{-}Co)_2B$. Exact compositions of these phases in the completely crystallized sample are found to be α–$(Fe_{0.7}Co_{0.3})$ and $(Fe_{0.3}Co_{0.7})_2B$.
**Keywords:** Crystallization, Mossbauer Spectroscopy, Electrical Resistivity, Differential Scanning Calorimetry, Activation Energy, X-ray Diffraction and Transmission Electron Microscopy.

## I. Introduction

Iron-rich metallic glasses prepared by rapid quenching technique are usually excellent soft ferromagnets, and have become technologically important materials [1,2]. Heat treatment of these glasses produces relaxation effects via annealing of quenched-in defects and internal stresses, and through changes in topological and chemical short-range orders. Therefore, the properties like Curie temperature($T_c$), Saturation magnetization($M_s$), Electrical resistivity(ρ) etc., tend to show dependence on the past thermal history of the glassy alloy. The lesser this dependence, better the thermal stability of the glassy alloy. Further, heating at high temperatures induces crystallization and transforms the material irreversibly into a more stable state, making the alloy brittle. Resulting crystalline phases not only depend upon the composition of the alloy but also on the details of the thermal treatment given. Therefore, investigation on the thermal behavior of the metallic glasses is important from basic as well as practical point of view.

Amorphous $Fe_{74}Co_{10}B_{16}$ (S1) and $Fe_{67}Co_{18}B_{14}Si_1$ (S2) alloys have relatively higher saturation magnetic induction($B_s$) among other commercially available metallic glasses and are considered to be important core materials for power transformers. In this paper, we report results on the thermal behaviour and crystallization of amorphous $Fe_{74}Co_{10}B_{16}$ (S1) and $Fe_{67}Co_{18}B_{14}Si_1$ (S2) alloys using various complementary techniques viz., Electrical Resistivity (ER), Differential Scanning Calorimetry (DSC), Low Field Magnetization (LFM), X-Ray Diffraction (XRD), Transmission Electron Microscopy (TEM) and Mossbauer Spectroscopy (MS). An attempt has been made to identify the morphology and crystalline phases in the crystallized sample using the last three techniques.

## II. Experimental

Amorphous $Fe_{74}Co_{10}B_{16}$ (S1) and $Fe_{67}Co_{18}B_{14}Si_1$ (S2) alloy ribbons were obtained from Allied Corporation, USA. Ribbons were approximately 25.4 mm wide and 30 μm thick. Sample for each measurement, as described below, were prepared by cutting pieces from 'as received' ribbons having appropriate geometry. Electrical resistivity(ρ) measurements were performed using the standard four probe method. DSC measurements were carried out using Perkin-Elmer calorimeter DSC – 1 under purified Helium gas atmosphere operating at constant heating rates. LFM measurements were carried out using PAR Vibrating Sample Magnetometer (VSM) model 155 in a dc magnetic field of 36 Gauss.

X-ray diffraction studies were carried out on a Philips PW1380 Horizontal diffractometer using Co-Kα radiation. For TEM studies, a Philips EM300 microscope operating at 100 kV was employed. Samples undergoing constant heating were immediately removed at the desired temperatures, and quenched in distilled water followed by quick air drying. Mossbauer measurements were performed using an Elscint Mossbauer spectrometer with one year old 25 mci $^{57}Co$ source in Rhodium matrix.

Spectra were recorded in the standard transmission geometry. Further, details of Mossbauer measurements may be found elsewhere [1 - 5].

The temperature at the sample in the measurements of LFM and MS was sensed using calibrated chromel-alumel thermocouple. Since, the location of the sensor was not quite exactly on the sample itself, the actual sample temperature was estimated to be no more different than 5 K in the temperature range 300 K < T < 1000 K for each experimental set up.

The temperature at the sample in the resistivity set up was found to be the most accurate representation of the actual sample temperature. To assess the reliability of the data, measurements were repeated at least on two specimens obtained from different batches of the ribbon. In each case, measurements were found to be reproducible within experimental accuracy.

## III. Results and Discussion

**Electrical Resistivity (ER)**

The electrical resistivity(ρ) of 'as received' amorphous $Fe_{74}Co_{10}B_{16}$ (S1) and $Fe_{67}Co_{18}B_{14}Si_1$ (S2) alloys was measured in the temperature range 80 K – 900 K. Fig.1(a) and Fig.1(b) show the resistivities of samples S1 and S2 as a function of temperature. As shown in Fig.1(a) and Fig. 1(b), the electrical resistivity ρ(T) of the samples S1 and S2, varies linearly from room temperature to the onset of crystallization. The onset of crystallization for S1 S2 samples takes place at ≈ 620 k and ≈ 660 K, respectively, as observed by a drop in the resistivity around these temperatures. Another sharp drop in ρ(T) is seen at 720 K for S1 and at 765 K for S2, indicating that the crystallization is taking place in a two step process. The variation of resistivity at high temperatures is linear. Similarly, Figure 2 displays the temperature dependence of Δρ/ρ(300) of the sample S2. Here, Δρ = ρ(T) – ρ(300) where ρ(T) and ρ(300) are the resistivities of the sample at temperatures T and 300 K, respectively. Δρ/ρ(300) of the sample shows a linear temperature dependence having a constant slope from 300 K to approximately 600 K with a slope change around 550 K. This slope change gives the first indication of thermally induced relaxation process leading to the possible onset of a partial crystallization of the amorphous matrix. A further increase in temperature results in a sharp drop in Δρ/ρ(300) at T = 665 K indicating fast crystallization. Examining the data points in Fig. 1(b) and Fig. 2, it seems that this crystallization process is about get completed between 755 K and 765 K as observed by the slight rounding of the data points in this temperature interval but soon another steeper drop in Δρ/ρ(300) takes place at 765 K and Δρ/ρ(300) reaches the minimum value at T = 785 K. About 785 K, Δρ/ρ(300) starts increasing linearly with rise in temperature. The rate of change of Δρ/ρ(300) about 785 K is constant, positive and steeper. This is indicative of a good metallic behavior of the completely crystallized sample. The resistivity data clearly indicates partial crystallization of the amorphous matrix at and above T ≈ 550 K. However, the volume fraction of the crystallites must be extremely small and these crystallites must be well isolated from each other electrically so as not to affect ρ vs T behavior of the sample appreciably. The possibility is that either α –Fe or α –(Fe-Co) alloy crystallites begin to nucleate first. Fig. 1(b) and Fig. 2 indicate that the actual crystallization of the amorphous matrix takes place in two-step process, the first one starting at T ≈ 665 K, and the second one starting at T ≈ 765 K. Further, the slope of either ρ vs T or Δρ/ρ(300) vs T curve in the temperature range 765 K – 785 K is much larger than that in the temperature interval 665 K – 750 K indicating that the second crystallization process is more catastroscopic than the first one. This suggests that during the first crystallization process while α –Fe or α –(Fe-Co) alloy is precipitating, either enough amorphous matrix is left in the sample or precipitation of yet another phase like Fe-Co-B is taking place and α –Fe or α –(Fe-Co) precipitate is possibly embedded in it. As it will be shown later, the possibility is that a $(Fe\text{-}Co)_3B$ phase pricipitates which decomposes at T = 765 K into α –(Fe-Co) and $(Fe\text{-}Co)_2B$ phases resulting in metallic short circuiting of the sample by α –$(Fe_{1-X}\text{-}Co_X)$ alloy. Thus, the resistivity data clearly shows structural changes taking place in amorphous $Fe_{67}Co_{18}B_{14}Si_1$ alloy at 550 K, 665 K, 765 K and 780 K. Further, it clearly establishes that this amorphous alloy crystallizes in a two-step process. Figure 1(b) also shows the cooling curve of the crystallized sample where the resistivity of the crystallized sample decreases almost linearly with decrease in temperature. Table 1 shows the Curie temperature($T_c$), First step Crystallization temperature($T_{x1}$), Second step Crystallization temperature($T_{x2}$), Room temperature resistivity ρ (300), Temperature coefficient of resistance(TCR), α and Debye temperature($\theta_D$) of the samples S1 and S2, respectively. From Table 1, it is clear that the resistivity and Debye temperatures decrease whereas the temperature coefficient of resistance increase when we move from sample S1 to sample S2.

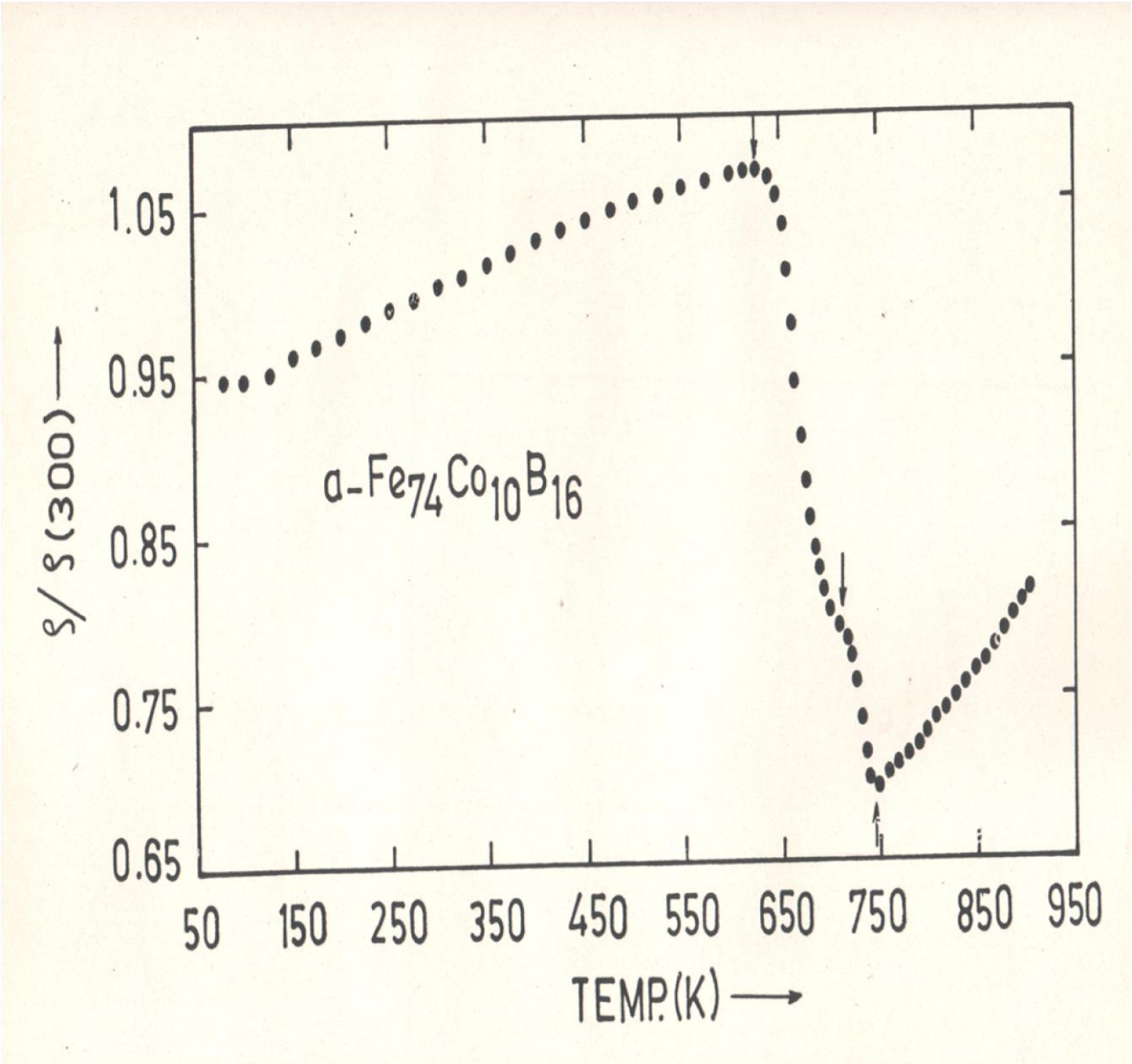


**Figure 1(a) Reduced resistivity, ρ/ρ(300) versus Temperature (K) of amorphous $Fe_{74}Co_{10}B_{16}$ alloy**

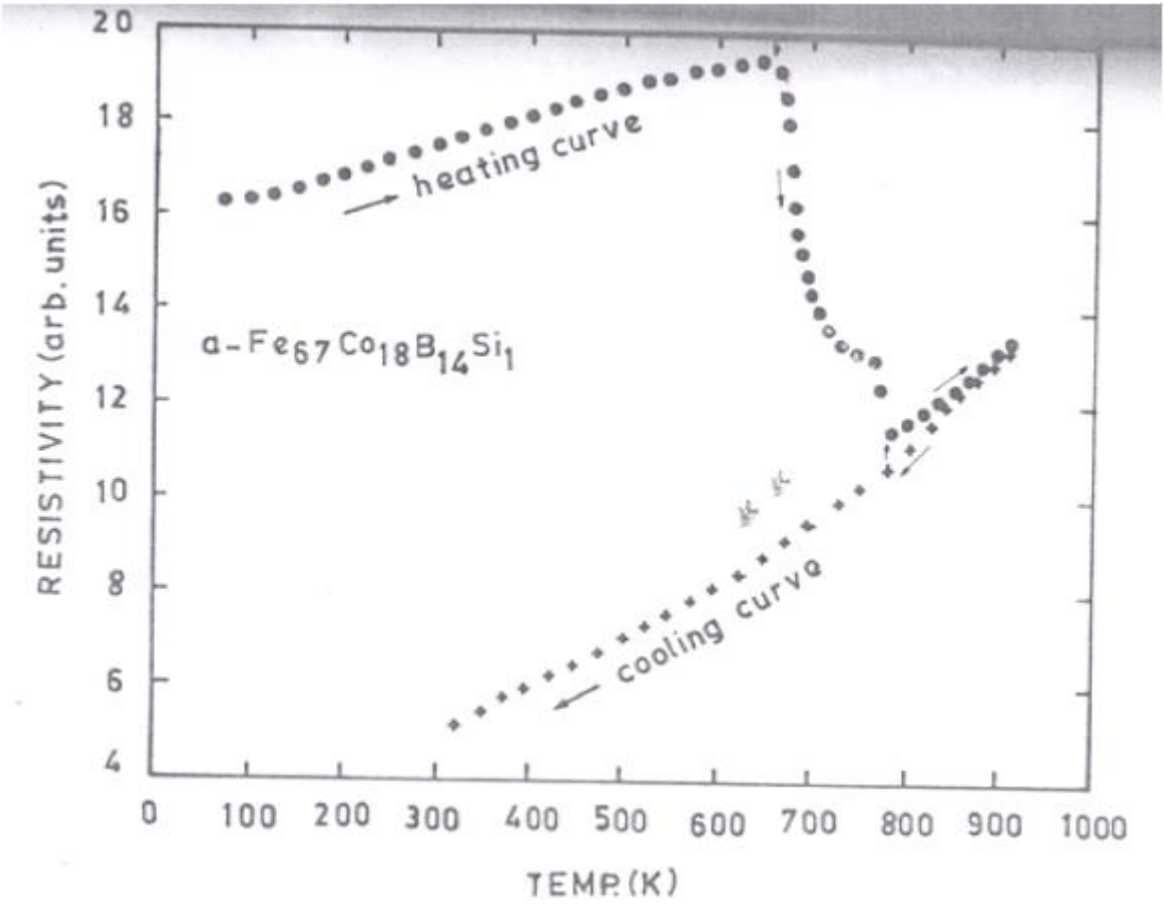


**Figure 1(b) Resistivity versus Temperature of amorphous $Fe_{67}Co_{18}B_{14}Si_1$ alloy**

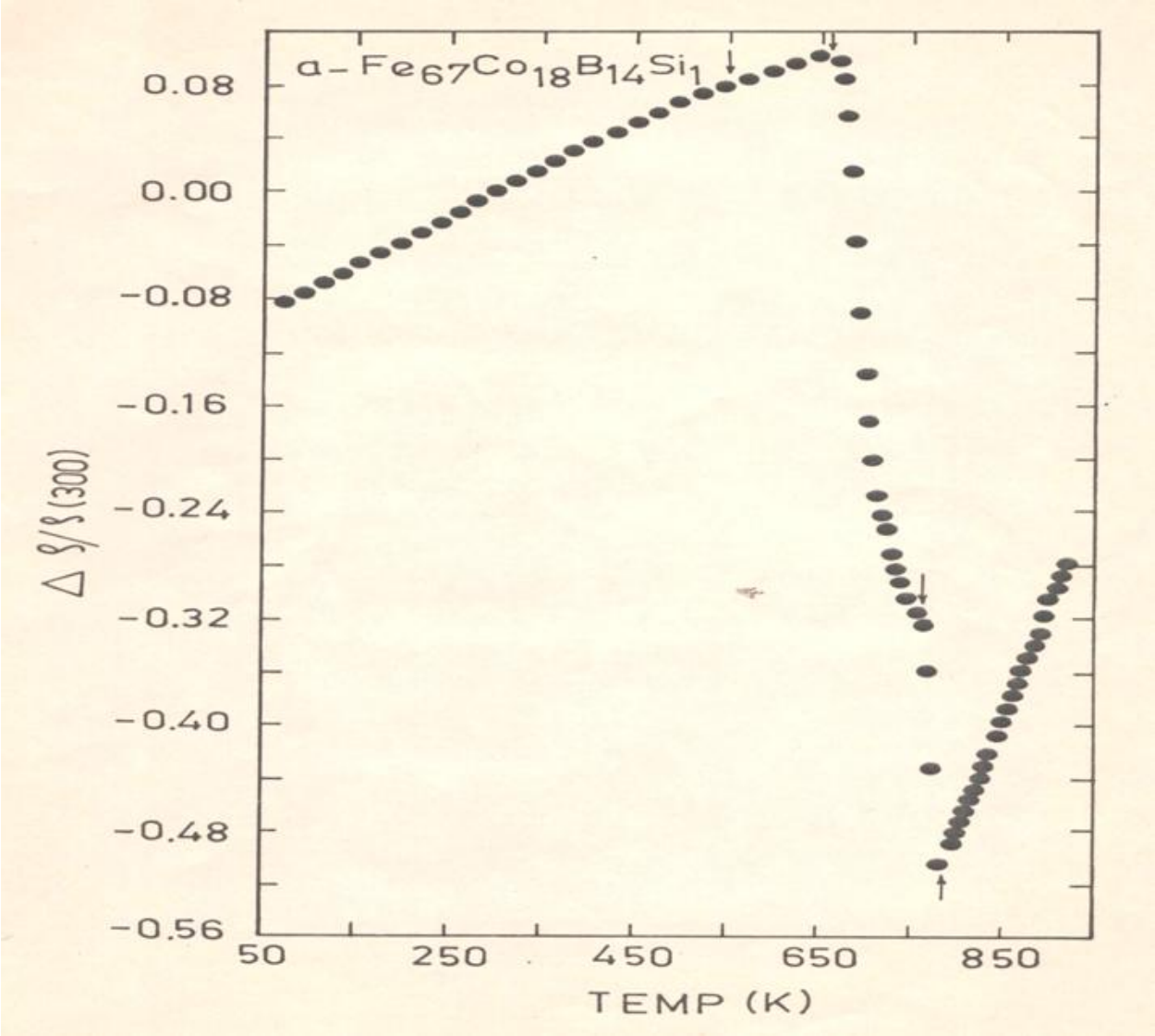


**Figure 2 Reduced fractional change of resistivity, Δρ/ρ(300) versus Temperature (K) of amorphous $Fe_{67}Co_{18}B_{14}Si_1$ alloy**

**Table 1**

**Curie temperature($T_c$), First step Crystallization temperature($T_{x1}$), Second step Crystallization temperature($T_{x2}$), Room temperature resistivity ρ (300), Temperature coefficient of resistance(TCR), α and Debye temperature($\theta_D$) of amorphous $Fe_{74}Co_{10}B_{16}$ and $Fe_{67}Co_{18}B_{14}Si_1$ alloys**

| Alloy system | $T_c$(K) (±2) | $T_{x1}$(K) (±2) | $T_{x2}$(K) (±2) | ρ (300) (μΩ -cm) | α ($10^{-5}K^{-1}$) | $\theta_D$(K) (±100) |
|---|---|---|---|---|---|---|
| $Fe_{74}Co_{10}B_{16}$ | 760 | 698 | 770.5 | 206.2 | 27.9 | 505 |
| $Fe_{67}Co_{18}B_{14}Si_1$ | 830 | 655 | 780 | 114.9 | 36.7 | 462 |

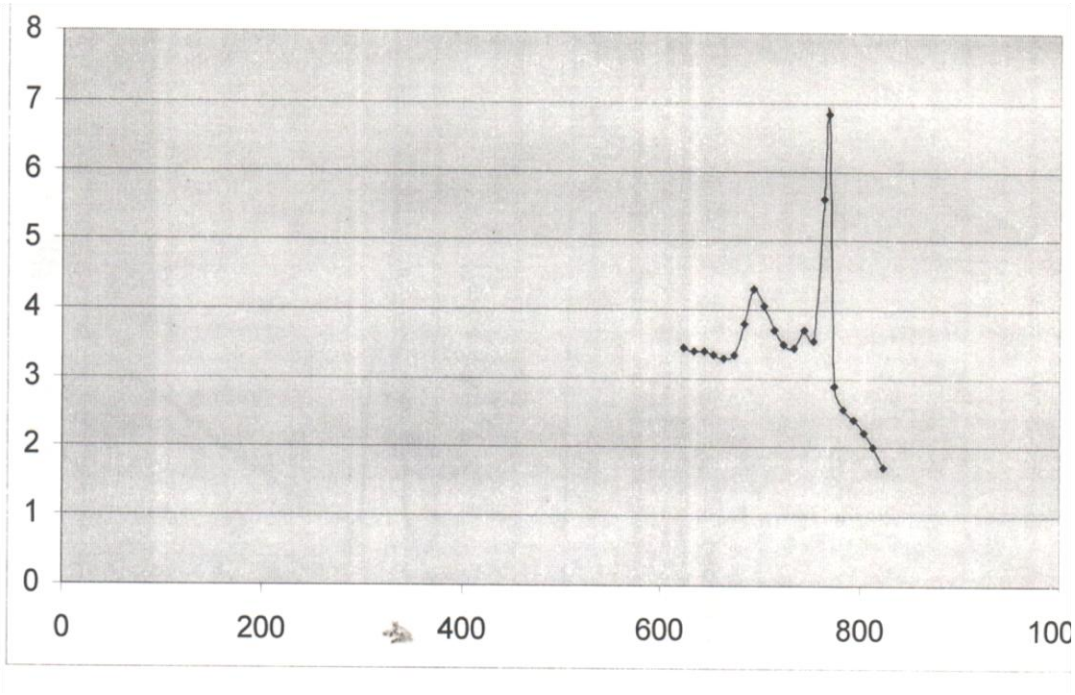


**Figure 3(a) Differential Scanning Calorimetry(DSC) curve of amorphous $Fe_{74}Co_{10}B_{16}$ (S1) alloy in the temperature range 610 K – 810 K.**

**Differential Scanning Calorimetry (DSC)**

Figures 3(a), 3(b) and 3(c) display the DSC curves of amorphous $Fe_{74}Co_{10}B_{16}$ (S1) and $Fe_{67}Co_{18}B_{14}Si_1$ (S2) alloys for the heating rate 5 K/min. Two exothermic peaks were observed in each case confirming the two-step crystallization process of the sample. Different heating rates of the amorphous sample do affect DSC thermograms. Thus, changes in the heating rate seems to influence the crystallization behavior. Such changes appear reasonable since change in the heating rate will alter the structural relaxation process and hence, the crystallization temperature, in turn, will be affected. It is also observed that the second peak is much sharper and higher than the first peak. This further confirms that the first crystallization process is more sluggish while the second one is very fast and catastrophic as already concluded by the electrical resistivity measurements. Further, the temperatures at which maximum of each peak in DSC thermograms appear, are in agreement with the two crystallization temperatures, $T_{x1}$= 665 K and $T_{x2}$ = 765 K, obtained by resistivity measurements. The suggested feeble partial crystallization of the sample at 550 K by electrical resistivity data is not indicated in the DSC thermograms because the heat involve in such a process is probably negligible and hence, is not detected.

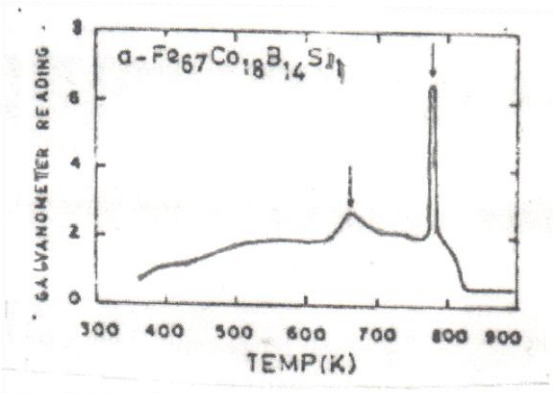


**Figure 3(b) Differential Scanning Calorimetry(DSC) curve of amorphous $Fe_{67}Co_{18}B_{14}Si_1$ (S2) alloy in the temperature range 300 K – 900 K.**

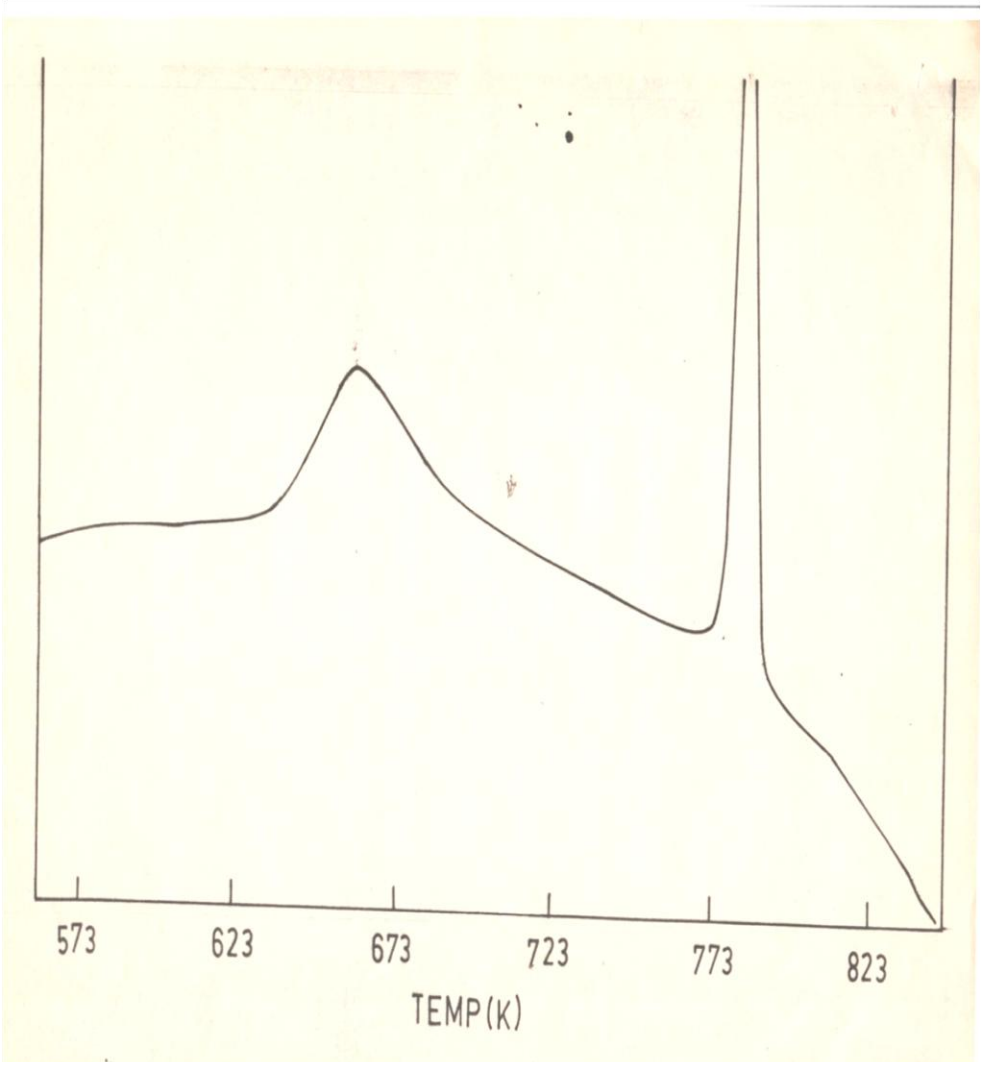


**Figure 3(c) Differential Scanning Calorimetry(DSC) curve of amorphous $Fe_{67}Co_{18}B_{14}Si_1$ (S2) alloy in the temperature range 570 K – 830 K**

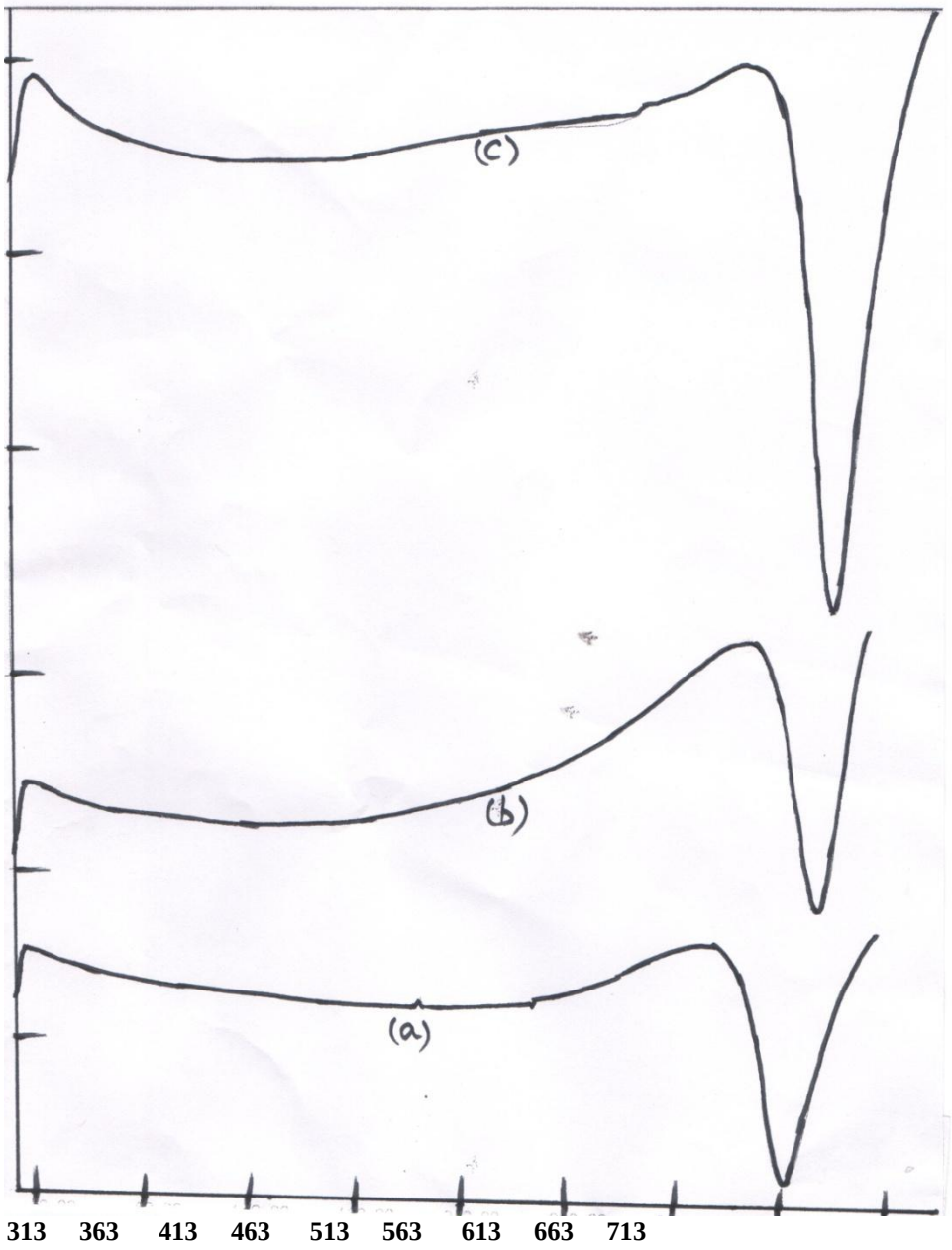


**Figure 4 Differential Scanning Calorimetry(DSC) curves of amorphous $Fe_{67}Co_{18}B_{14}Si_1$ (S1) alloy at the heating rates $10^0$C/min(a), $30^0$C/min(b) and $50^0$C/min(c), respectively for the First Peak.**

Figure 4 shows the first endothermic peak of DSC curves of amorphous $Fe_{67}Co_{18}B_{14}Si_1$ alloy **(S1)** at the heating rates $10^0$C/min(a), $30^0$C/min(b) and $50^0$C/min(c), respectively.

The activation energy ($E_c$) for crystallization of an amorphous alloy under a linear heating rate (non-isothermal) is calculated using Masutika-Sakka, Augis-Bennet and Kissinger methods [6, 7, 8, 9], which relates the peak temperature ($T_p$) with heating rate ($\alpha$) using the relations.

$$\ln \alpha = -[E_c/(RT_p)] + \text{Constant} \quad \ldots\ldots\ldots\ldots\ldots\ldots\ldots\ldots\ldots(1)$$

$$\ln (\alpha/T_p) = -[E_c/(RT_p)] + \text{Constant} \quad \ldots\ldots\ldots\ldots\ldots\ldots\ldots\ldots\ldots\ldots(2)$$

$$\ln (\alpha/T_p^2) = \text{Constant} - [E_c/(RT_p)] \quad \ldots\ldots\ldots\ldots\ldots\ldots\ldots\ldots\ldots\ldots(3)$$

where 'R' is Gas constant.

**Table 2**
**Heating rate, First peak temperature of amorphous $Fe_{67}Co_{18}B_{14}Si_1$ alloy**

| S. No. | Heating Rate ($^0$C/min) | First peak temperature ($^0$C/min) |
|---|---|---|
| 1 | 10 | 392.0 |
| 2 | 30 | 410.3 |
| 3. | 50 | 420.7 |

**Table 3**
**Activation energy of crystallization ($E_c$), in kJ/mol, of amorphous $Fe_{67}Co_{18}B_{14}Si_1$ alloy calculated from non-isothermal methods.**

| | Matusita-Sakka's Method | Augis-Bennet's Method | Kissinger's Method | Average Value |
|---|---|---|---|---|
| Peak1 | 220 | 208 | 205 | 211 |

Table.2 shows the heating rate, first peak temperature of amorphous $Fe_{67}Co_{18}B_{14}Si_1$ alloy.
The values of $\mathbf{E_c}$ obtained for the present sample using the above three methods are given in Table 3. Comparison of the $\mathbf{E_c}$ values obtained for different non-isothermal methods shows that the $\mathbf{E_c}$ values are in good agreement with other similar systems [3]. This means that one can use any one of the three methods to calculate the activation energy of crystallization.

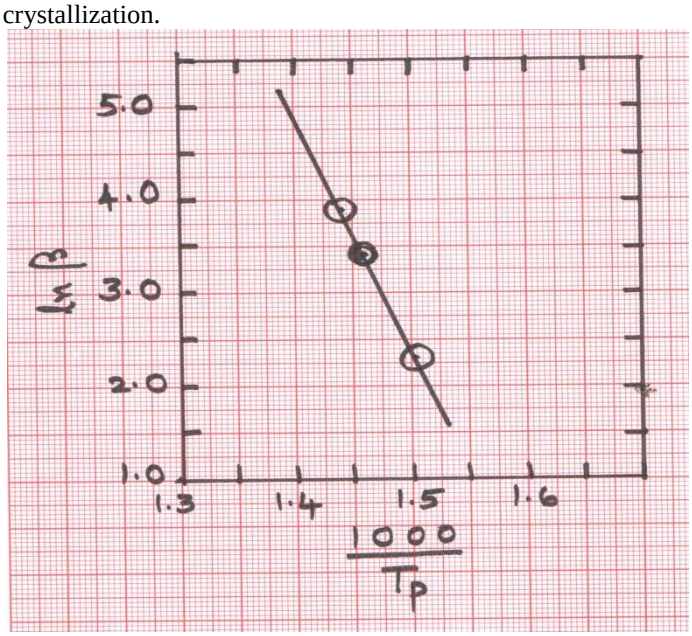


**Figure 5 Matusita - Sakka plot for amorphous $Fe_{67}Co_{18}B_{14}Si_1$ alloy**

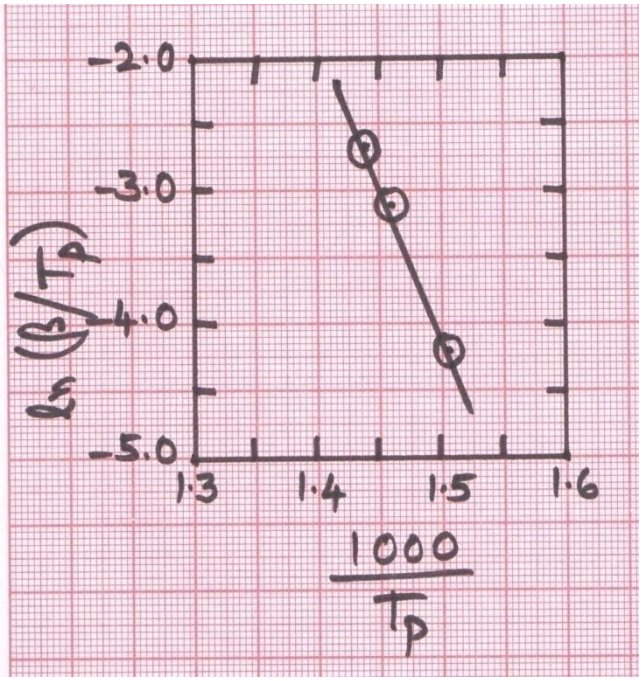


**Figure 6 Augis - Bennett plot for amorphous $Fe_{67}Co_{18}B_{14}Si_1$ alloy**

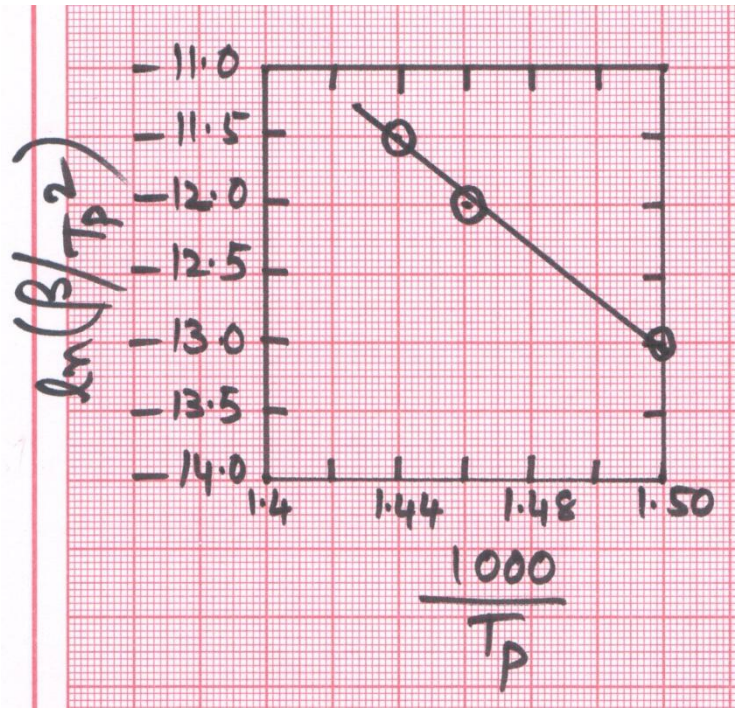


**Figure 7. Kissinger plot for amorphous $Fe_{67}Co_{18}B_{14}Si_1$ alloy**

Figures 5, 6 and 7 show the plots of Masutika-Sakka, Augis-Bennet and Kissinger methods for amorphous $Fe_{67}Co_{18}B_{14}Si_1$ alloy.

**Low Field Magnetization (LFM)**

While the resistivity and the DSC results establish the details of crystallization processes, the magnetic thermogram gives information about the magnetic nature of the crystallized products. Thermomagnetic behavior of amorphous $Fe_{67}Co_{18}B_{14}Si_1$ alloy was investigated
by measuring magnetization(M) of the sample in a dc magnetic field of 36 Gauss using VSM. Thus, Fig. 8 shows the Magnetization (M) curve of amorphous $Fe_{67}Co_{18}B_{14}Si_1$ alloy with temperature (K). As in Fig. 8, from 300 K, the magnetization of the sample decreases very slowly upto 580 K. However, at just above 580 K, the magnetization of the sample starts increasing indicating precipitation of some magnetic component in the alloy. This is in line with the resistivity changes at about 550 K as already discussed. The Magnetization of the sample becomes constant at approximately 665 K, and a further rise in sample temperature shows a decrease in M again upto 790 K and then starts decreasing upto 900 K, the maximum temperature reached in the experiment.

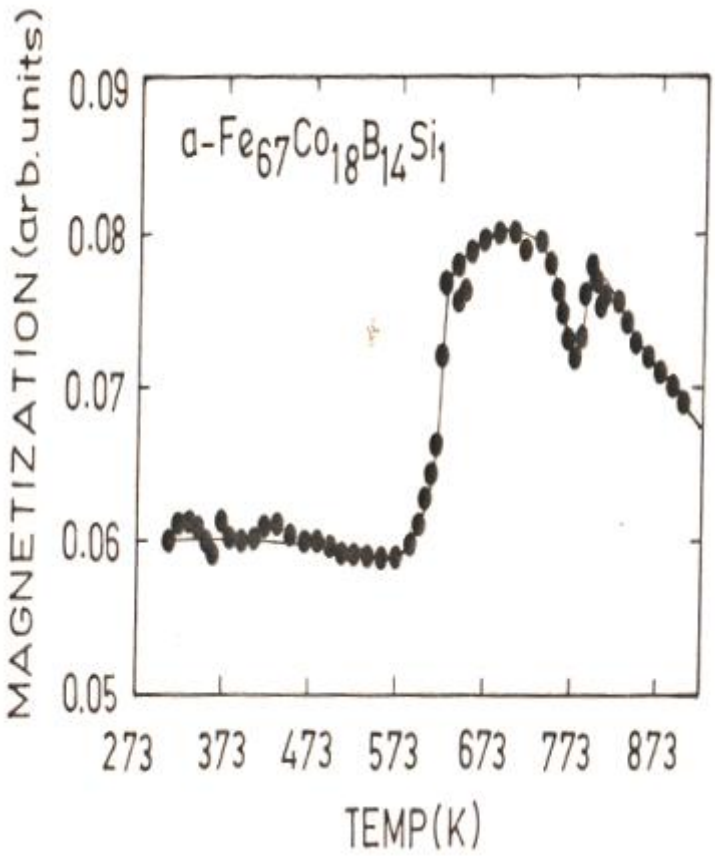


**Figure 8 Magnetization(M) versus Temperature(T) curve of amorphous $Fe_{67}Co_{18}B_{14}Si_1$ alloy**

The following conclusions could be drawn from Fig. 8.

1. The magnetization of the sample rapidly increases from approximately 573 K to approximately 673 K, indicating the primary(first step) crystallization of the sample,
   which reflects in a rapid decrease in the resistivity of the sample with increase in the temperature (Fig. 1b and Fig. 2). A broad peak is observed in the DSC of the sample between 573 K and 673 K (Fig.3b and 3c).

2. From 773 K to approximately 783 K, the magnetization of the sample increases sharply indicting the secondary(second step) crystallization of the sample, which also reflects in the sudden drop in the resistivity of the sample with increase in temperature(Fig. 1b and Fig. 2). A sharp peak is observed in the DSC of the sample in this temperature range. (Fig.3b and 3c).
3. At 790 K, the crystallization process is complete, and the measured M, which is total magnetization of all the crystallized products, decreases with increase in temperature.
   This reflects in the increase in the resistivity of the crystallized sample with temperature as shown in Figs. 1b and 2.

4. The Crystallization temperature ($T_x$) of amorphous $Fe_{67}Co_{18}B_{14}Si_1$ alloy is smaller than its Curie temperature ($T_c$) which is a general tendency of cobalt containing samples(Table 1).

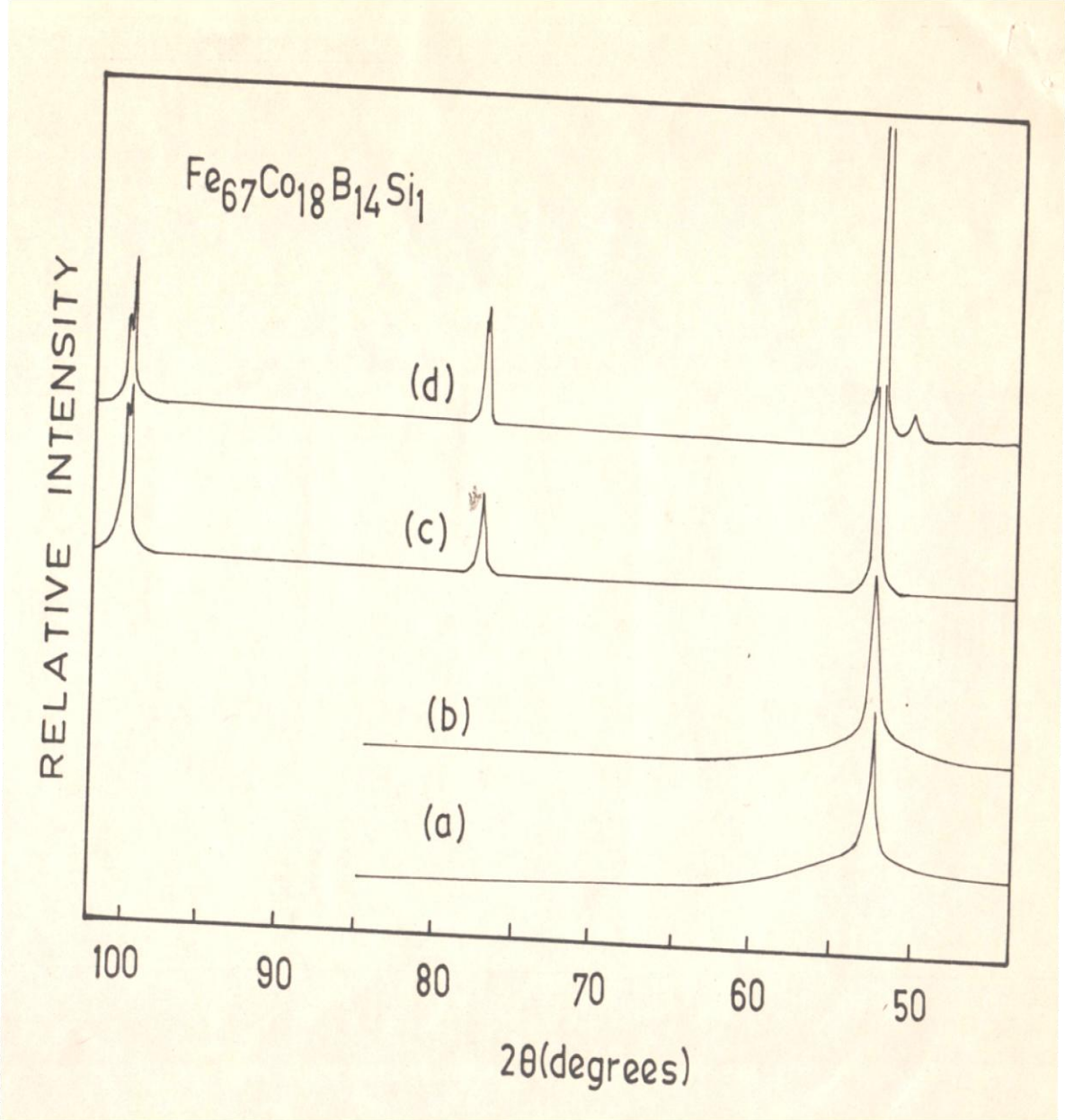


**Figure 9 X-ray diffractometer scan of the 'as received' sample of amorphous $Fe_{67}Co_{18}B_{14}Si_1$ alloy(S2) samples after different heat treatments. i.e., (a) 300 K, (b) 650 K, (c) 800 K and (d) 900 K.**

**X-Ray and TEM**

Figure 9 shows the X-ray diffractometer scan of the 'as received' sample of amorphous $Fe_{67}Co_{18}B_{14}Si_1$ alloy (S2) and samples after different heat treatments. Another batch of as received sample shows the crystalline peak corresponding to α –Fe phase superimposed over a broad maxima. Thus, it is clearly evident that the α –Fe crystallites are uniformly distributed within the amorphous matrix, all along the sample length and may not be confined to the surface layer only [10]. TEM results as described below, also support the present observations. For samples heated to higher temperatures, relative crystalline peak intensity of α –Fe becomes larger suggesting that more and more of α –Fe is precipitating out from the amorphous matrix. Samples heated upto 800 K [Fig. 9(c)] and 900 K [Fig. 9(d)] show additional peaks corresponding to $Fe_2B$. However, an exact solution as to which phase is present seems to be very difficult from the existing data. Presence of Co(18 wt. %) favours a solid solution Fe-Co and hence lattice parameters or d-spacing change. These changes are very small and are difficult to be detected with the present experimental accuracy using X-rays.

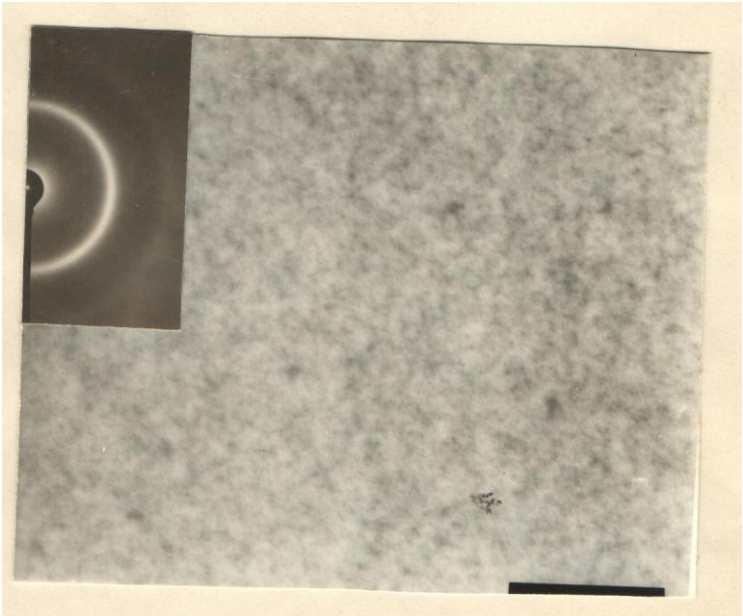

**Figure 10 TEM micrograph and SAD pattern of the 'as received' $Fe_{67}Co_{18}B_{14}Si_1$ alloy (S2) indicating amorphous structure.**

TEM studies were carried out essentially, to check the morphology of the crystalline products. Room temperature micrograph of amorphous $Fe_{67}Co_{18}B_{14}Si_1$ alloy(S2) shows structureless features (Fig. 10) and a Selected Area Diffraction (SAD) pattern of the same area shows halo rings (Fig. 10). Contrast observed in Fig. 10 is due to etching effects during electropolishing of the specimen which is not uncommon of the amorphous alloy. In localized regions within the sample, regularly distributed crysytallites have been observed. Thus, Fig. 11(a) and Fig. 11(b) show the bright field and dark field images of those regions of the 'as received' sample along with the associated SAD pattern. Upon heating the amorphous sample(S2) to 650 K, the amorphous matrix begins to crystallize. Thus, Fig. 12 shows the TEM micrograph and SAD pattern of the sample S2 heated to 650 K.

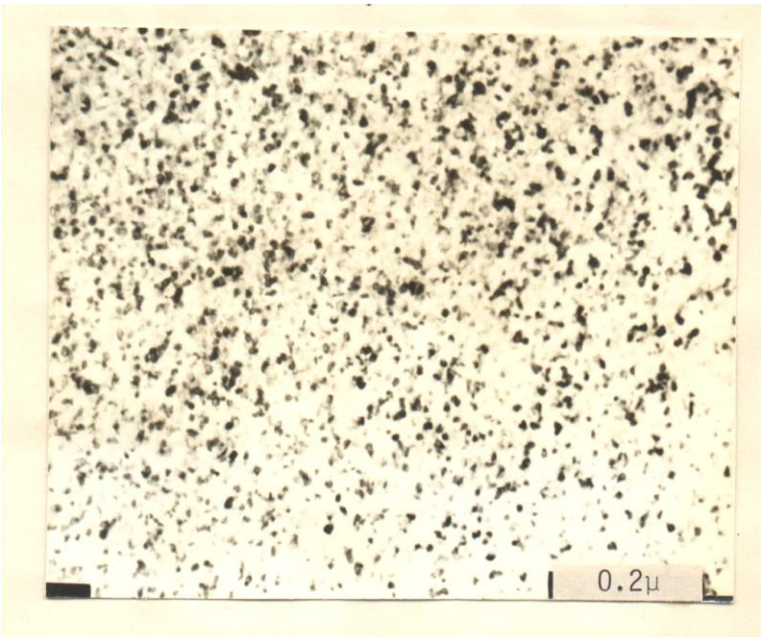


**Figure 11(a) Bright field image of the 'as received' $Fe_{67}Co_{18}B_{14}Si_1$ alloy (S2) along with SAD pattern.**

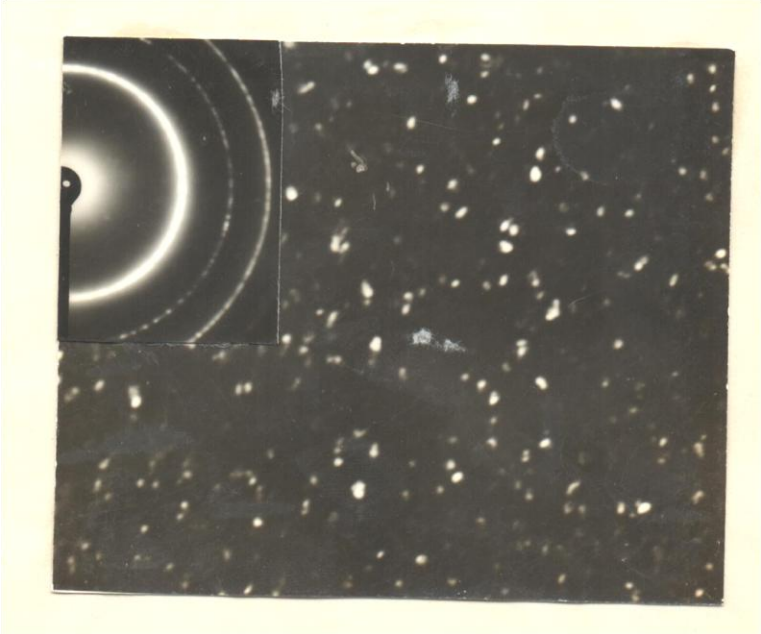

**Figure 11(b) The dark field picture formed from the inside ring of SAD corresponding to Fig. 11(a).**

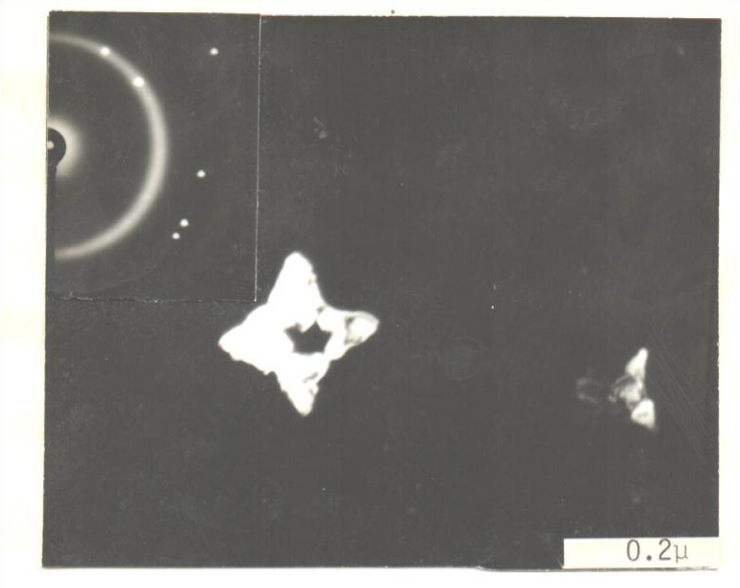


**Figure 12 TEM micrograph and SAD pattern of amorphous $Fe_{67}Co_{18}B_{14}Si_1$ alloy (S2) heated to 650 K.**

**Figure 13(a) TEM micrograph showing Dendritic α –Fe crystals in an amorphous matrix of amorphous $Fe_{67}Co_{18}B_{14}Si_1$ alloy (S2) heated to 670 K.**

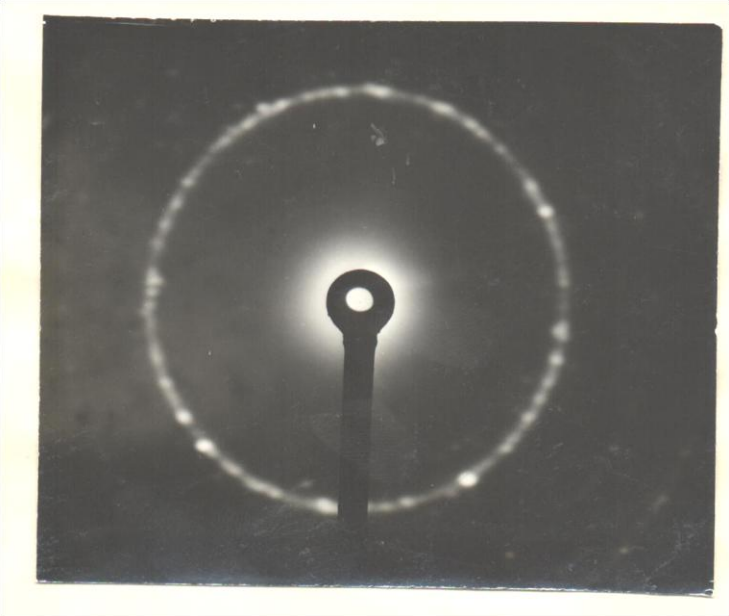

**Figure 13(b) The SAD pattern of Fig. 13(a).**

For the sample heated to 670 K, Electron micrograph and the corresponding SAD pattern are shown in Fig. 13 (a) and 13(b). Fig. 13 (a) shows the precipitation of α –Fe and $Fe_2B$ phases. The presence of fine dendrite like crystallites as shown in Fig. 13(a) is identified as α –Fe.

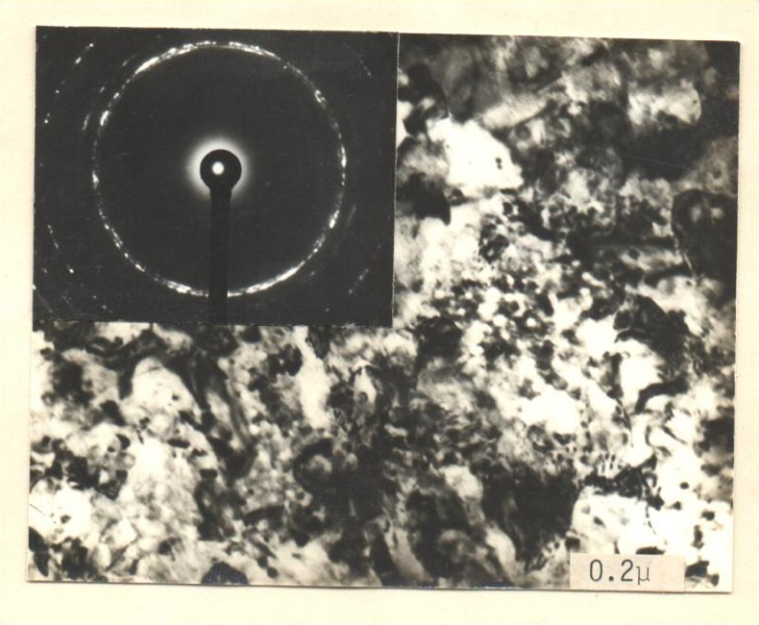


**Figure 14 Complete crystallization of the amorphous matrix of amorphous $Fe_{67}Co_{18}B_{14}Si_1$ alloy (S2) heated to 800 K with SAD pattern.**

Amorphous $Fe_{67}Co_{18}B_{14}Si_1$ alloy (S2) heated up to 800 K showed complete crystallization of the amorphous matrix as shown in Fig. 14 which shows precipitated α –Fe phase having an average grain size of 3.5 μm and a lattice parameter of 2.866 Å as evident from X-ray analysis. Figure 14 also shows the morphology and the corresponding SAD pattern of the crystallized specimen showing the presence of $Fe_2B$ phase.

**Mossbauer Spectroscopy (MS)**

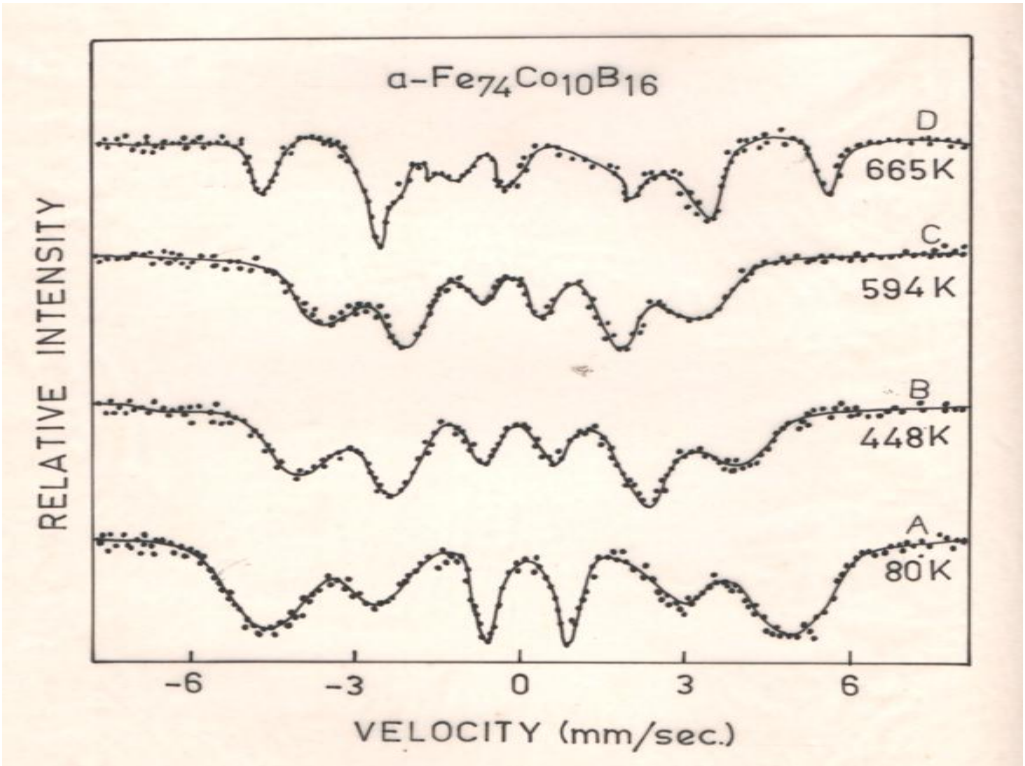


**Figure 15 Mossbauer spectra of amorphous $Fe_{74}Co_{10}B_{16}$ alloy (S1) at various temperatures**

The $^{57}$Fe Mossbauer Spectroscopy (MS) is a very useful microscopic technique to study hyperfine interactions and local atomic structural properties of iron-rich metallic glasses, and has been extensively applied to investigate these materials [1,2,4,5]. This technique is very sensitive to the local environment and interactions as seen by the $^{57}$Fe Mossbauer nuclei. This technique has been applied to investigate thermally induced changes in amorphous $Fe_{74}Co_{10}B_{16}$ (S1) and $Fe_{67}Co_{18}B_{14}Si_1$ (S2) alloys and in this section, results concerning crystallization of the amorphous samples are presented. Thus, Fig. 15 shows the Mossbauer spectra of amorphous $Fe_{74}Co_{10}B_{16}$ alloy (S1) at various temperatures. Figure 16 shows the Mossbauer spectrum of the 'as received' $Fe_{67}Co_{18}B_{14}Si_1$ alloy (S2) sample at 300 K. The spectrum consists of broad and overlapping yet well resolved Zeeman split six-lines which are typical of iron-rich metallic glasses. The line-widths of the outermost lines are approximately 1.85 mm/sec which are about six and a half times larger than those of the room temperature Mossbauer spectrum of a thin α –Fe iron foil.

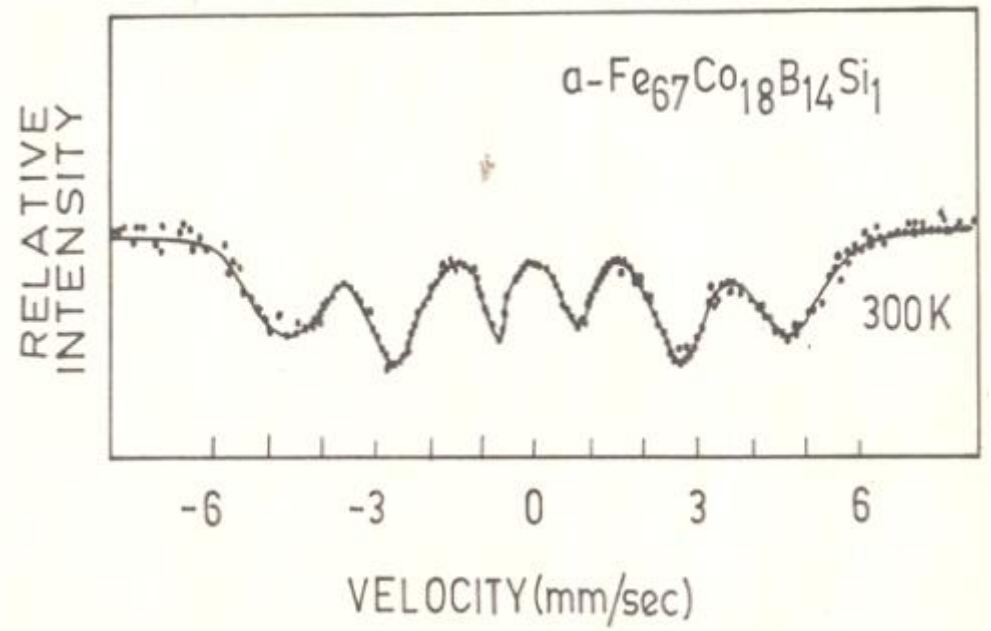


**Figure 16 Room temperature Mossbauer spectrum of 'as received' $Fe_{67}Co_{18}B_{14}Si_1$ alloy (S2)**

Mossbauer spectra of amorphous $Fe_{67}Co_{18}B_{14}Si_1$ alloy(S2) heated upto 601 K showed similar features as the one taken at 300 K indicating that the local atomic structure did not change appreciably. No changes characteristics of α –Fe or α –(Fe-Co) precipitated at $T \geq 550$ K or the precipitation was so small (less than 3%) that it could not be detected in the Mossbauer spectrum recorded at $T \geq 550$ K. The first indication of change in the Mossbauer Spectrum was observed at $T \approx 626$ K as shown in 17 (a) where outermost peaks show a slight splitting. The spectrum taken at 642 K as in Fig. 17(b) also showed the splitting having two more small symmetrical absorption lines at lower and higher values of the velocity respectively, producing a total of ten absorption lines. On further heating, first, third, eight and tenth lines grow in intensity. Second and ninth lines also seem to grow in intensity, but they strongly overlap with the third and eighth lines. The remaining four lines do not show any significant change in their positions and intensities. Thus, a total of eight lines appear in the Mossbauer spectrum at 650 K as shown in Fig. 17(c). Further, change in the spectrum is observed at 700 K as shown in Fig.17(d), the inner four lines become unresolved and Fig.17(e) shows the spectrum at 750 K where the inner four lines seem to have split into six or seven lines. Further, heating of the sample to 900 K shows more changes in the spectrum where eleven lines are easily seen as in Fig.18, but asymmetry of the other intense lines indicates that the spectrum is truly complex, i.e., there are more than eleven lines many of them overlap. However, the spectrum essentially remains un changed from 800 K to 900 K in the sample S2.

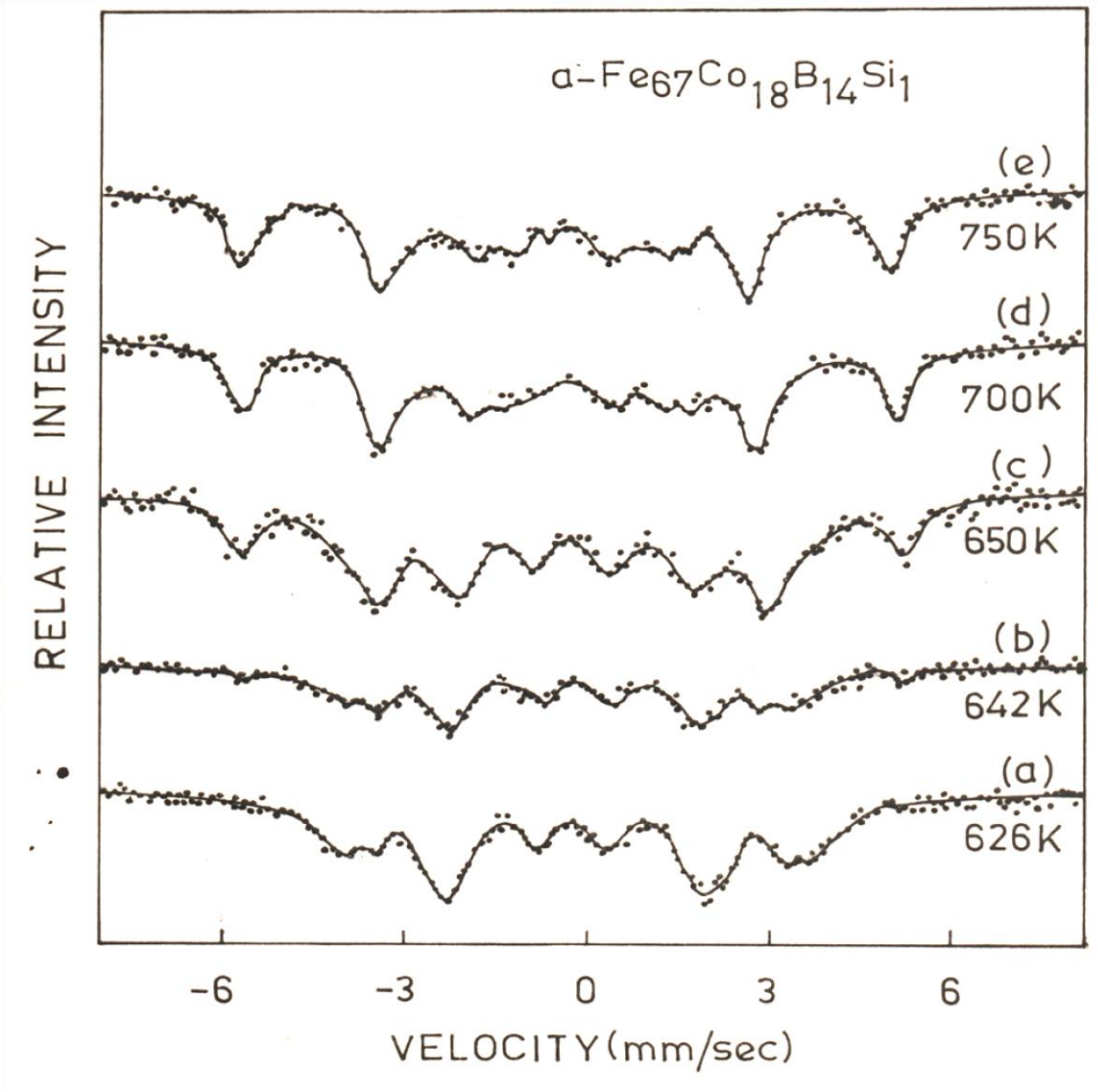


**Figure 17 Mossbauer spectra of amorphous $Fe_{67}Co_{18}B_{14}Si_1$ alloy (S2) at various temperatures**

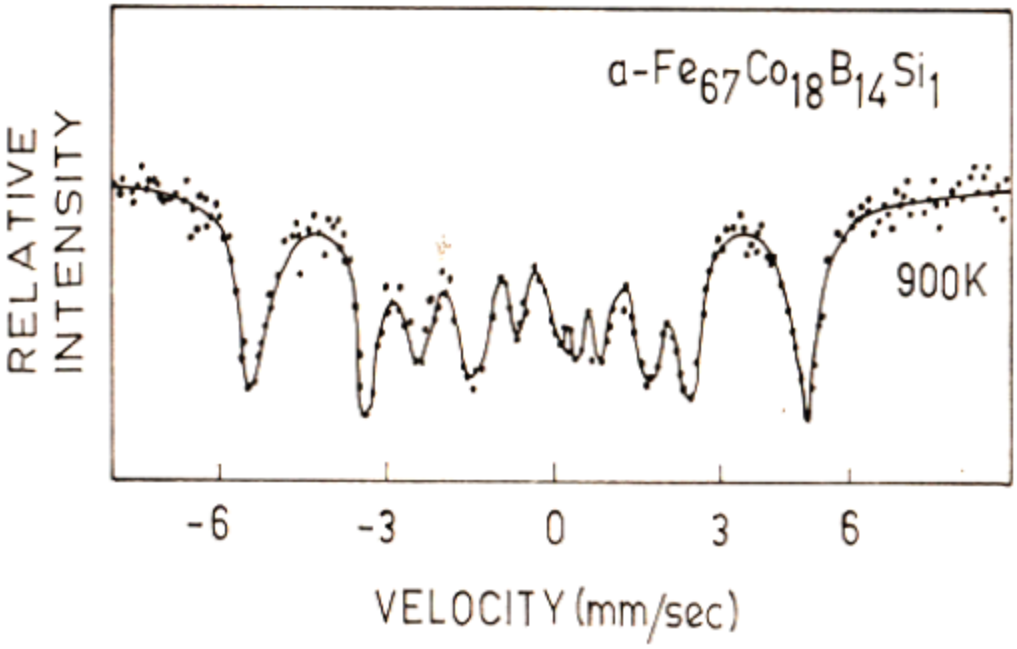


**Figure 18 Mossbauer spectrum of amorphous $Fe_{67}Co_{18}B_{14}Si_1$ alloy(S2) at 900 K.**

Figure 19(a) shows the room temperature Mossbauer spectrum of the amorphous $Fe_{67}Co_{18}B_{14}Si_1$ alloy(S2) which was used to record Mossbauer spectra at different temperatures upto 900 K. For comparison, 'as received' samples were heat treated at 855 K for 15 min and at 1130 K for 5 min in vacuum and immediately quenched to room temperature. Mossbauer spectra of these samples recorded at room temperature are shown in Figs. 19(b) and 19(c), respectively which do not show any significant change in the essential features. Considering the evolution of changes in the Mossbauer spectra as a function of temperature described above, the following suggestions are put forward for the crystallization mechanism of amorphous $Fe_{67}Co_{18}B_{14}Si_1$ alloy(S2). No changes in Mossbauer spectra are observed upto □ 600 K□ which could be correlated with the observed changes in the Electrical Resistivity (ER) and Low Field Magnetization (LFM) observations.

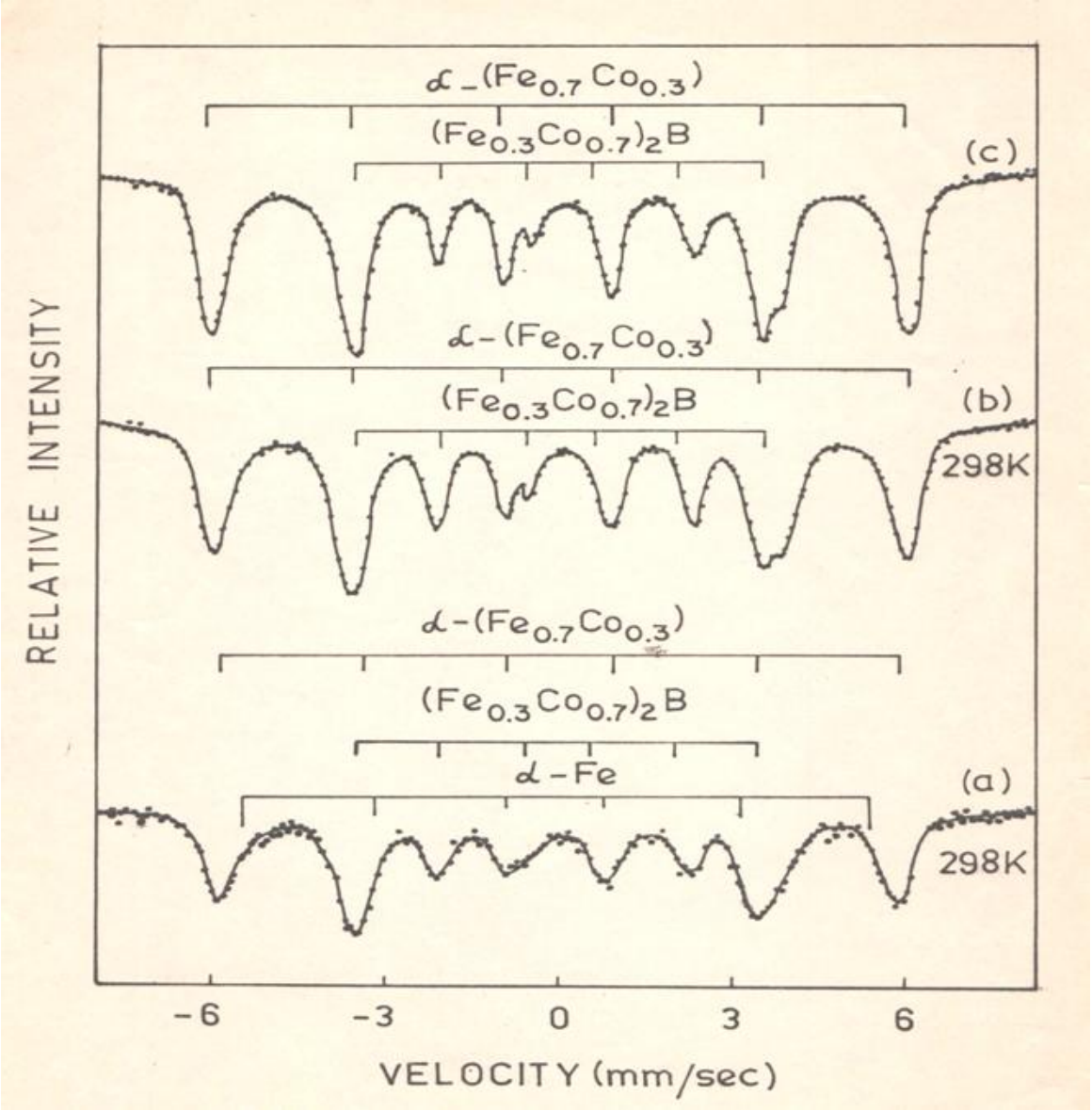


**Figure 19 Room temperature Mossbauer spectra of Crystallized $Fe_{67}Co_{18}B_{14}Si_1$ (S2) samples heat treated at various temperatures.**

This suggests that either no crystallization or precipitation of a magnetic phase containing iron takes place or even if it does, the amount is small enough not to be detected by the Mossbauer technique. The Mossbauer spectrum at 626 K showing a small splitting in the first and sixth peaks suggests the presence of a small amount of $(Fe\text{-}Co)_3B$ alloy which on further heating decomposes into α–(Fe-Co) and $(Fe\text{-}Co)_2B$, since at higher temperatures one sextet is identical to that of $(Fe\text{-}Co)_2B$ alloy. Appearance of new small peaks at lower and higher velocities are attributed to α–(Fe-Co) alloy. These peaks grow in intensity indicating more and more precipitation of α–(Fe-Co) alloy. Figure 19 shows a field of 363 k0e.

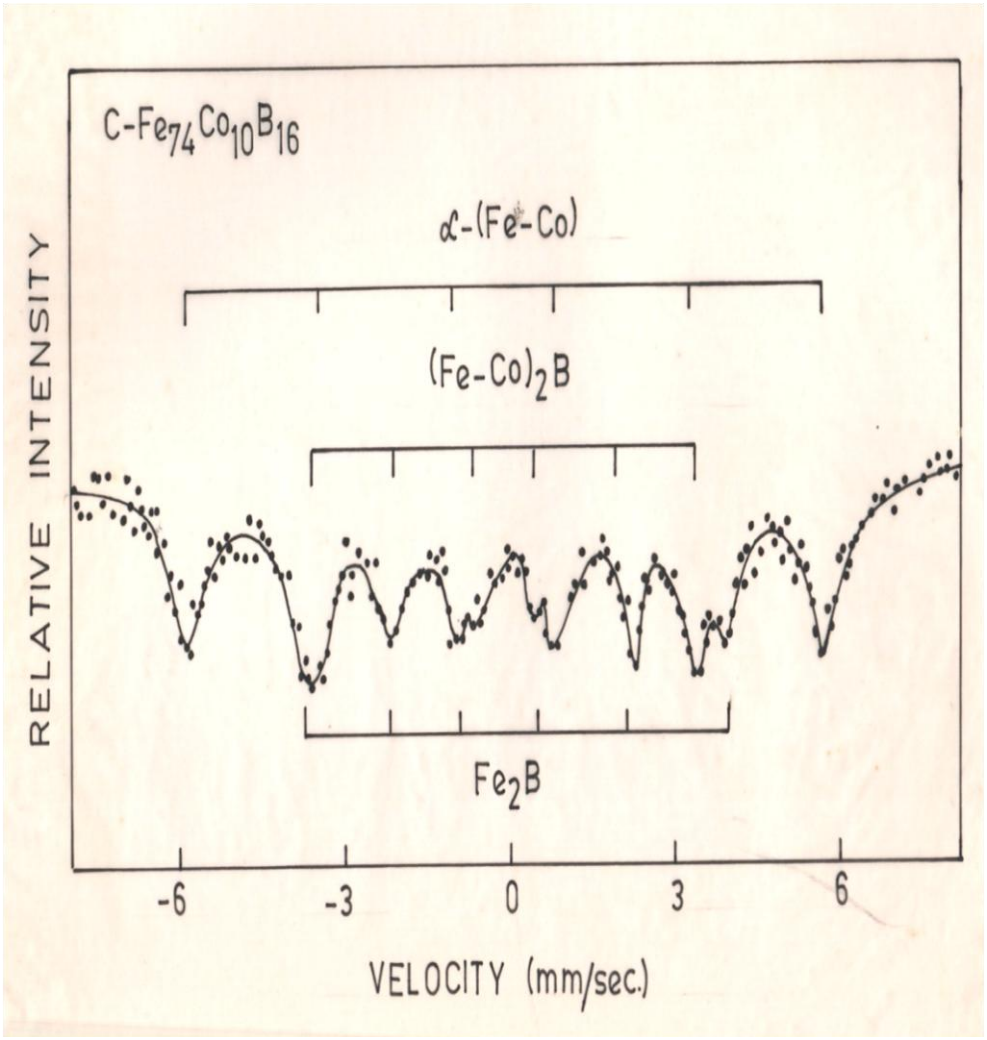


**Figure 20 Room Temperature Mossbauer spectrum of Crystallized $Fe_{74}Co_{10}B_{16}$ (S1) sample.**

Comparing this value with the work of Vincze et al [11] and Mayo et al [12], it could easily be estimated that in the present alloy the Fe-Co solid solution has an approximate concentration of $(Fe_{0.7}Co_{0.3})$. There seems to be no evidence of the presence of α–Fe precipitate as suggested by Choi et al [10]. Thus, the Mossbauer study of amorphous $Fe_{67}Co_{18}B_{14}Si_1$ alloy firmly establishes that one of the major crystalline products is α–(Fe-Co) and not α–Fe. What happens at 700 K is not exactly clear but a further decomposition of $(Fe\text{-}Co)_3B$ into α–(Fe-Co) and $(Fe\text{-}Co)_2B$ phases might be responsible for the observed effect since the later compound has small hyperfine field if Co content is higher. Thus, the Mossbauer spectra of completely crystallized samples clealy show a contribution from α–$(Fe_{0.7}Co_{0.3})$ and $(Fe_{0.3}Co_{0.7})_2B$ phases [11,12]. It is quite likely that contributions from some other magnetic phases may also present, because of observed asymmetries and small splittings in the lines. However, it was not possible to identify them as not much detailed work has been done on $(Fe\text{-}Co)_2B$ and (Fe-Co)B components except a few [13]. Similarly, the crystallized $Fe_{74}Co_{10}B_{16}$ (S1) shows a complex spectrum as shown in Fig. 20 in which α–(Fe-Co), $(Fe\text{-}Co)_2B$ and $Fe_2B$ phases are present.

**Conclusions**

The transformation from the metastable amorphous state to an equilibrium crystalline state in amorphous $Fe_{74}Co_{10}B_{16}$ (S1) and $Fe_{67}Co_{18}B_{14}Si_1$ (S2) alloys occurs through a two step crystallization process. The activation energy evaluated for the first peak of amorphous $Fe_{67}Co_{18}B_{14}Si_1$ alloy is in good agreement with other reported values of the similar compositions. LFM measurements show that the alloy remains ferromagnetic at least upto 900 K. Mossbauer, X-ray and TEM studies for 'as received' samples have clearly shown the uniformly distributed clusters of α–Fe microcrystals embedded in the amorphous matrix all along the sample length. Detailed analysis on the crystallized samples showed the composition of the grown phases as α–$(Fe_{0.7}Co_{0.3})$ and $(Fe_{0.3}Co_{0.7})_2B$.

**Acknowledgements**

The authors would like to thank the Management, Principal, Head of Sciences & Humanities and staff of M.V.S.R. Engineering College for continuous encouragement and support in completing the work.

**References**

[1] Bhanu Prasad B., Anil K. Bhatnagar and Jagannathan R., J. Non-Cryst. Solids **61-62** (1984) 391
[2] Bhatnagar A.K., Bhanu Prasad B. and Jagannathan R., Journal of Applied Physics, **57** (1985) 3514
[3] Prasad B.B. and Bhatnagar A.K., J. Magn. Magn, Mater., **31-34** (1983a) 1479
[4] Prasad B.B., Bhatnagar A.K., and Jagannathan R., Solid State Commun., **36** (1980) 661
[5] Prasad B.B., Bhatnagar A.K., and Jagannathan R., J. Appl. Phys., **54** (1983b) 2019
[6] Arun Pratap, Lilly Shanker Rao T., Kinnary Patel and Mukesh Chawda, Bull. Mat. Sci., **32 (**2009) 527
[7] Kissinger H.E, Anal. Chem., **29** (1957) 1702
[8] Lu W. Yang L., Yan B., Huang W. and Lu B., J. Alloys and Comp., **413** (2006) 85
[9] Kazumasa Matusika and Sumio Sakka, Bull. Instrum. Chem. Res., **59** (1981) 159
[10] Choi M., Pease D.M., Hines W.A., Budnick J.I., Hayes G.H., and Kabacoff L.T., J. Appl. Phys. **54** (1983) 4193
[11] Vincze I., Campbell I.A., and Meyer J., Solid State Commun. **15** (974) 1495
[12] Mayo B.D., Forester D.W. and Spooner S., J. Appl. Phys., **41** (1970) 1319
[13] Takacs L., Cadeville M.C. and Vincze I., J. Phys. F **5** (1975) 800